International Journal of GEOMATE, May., 2021, Vol.20, Issue 81, pp.8-15
ISSN: 2186-2982 (P), 2186-2990 (O), Japan, DOI: https://doi.org/10.21660/2021.81.Gx194
Geotechnique, Construction Materials and Environment

ESTIMATION OF SUBSURFACE STRUCTURE BASED ON MICROTREMOR AND SEISMIC OBSERVATIONS IN AREA DAMAGED BY 2018 HOKKAIDO EASTERN IBURI EARTHQUAKE, HOKKAIDO, JAPAN

* Tatsuya Noguchi[1], Isamu Nishimura[1], Yusuke Ono[1] and Masanori Kohno[1]

[1]Faculty of Engineering, Tottori University, Japan

*Corresponding Author, Received: 01 July 2020, Revised: 27 Nov. 2020, Accepted: 13 Feb.2021

ABSTRACT: To investigate the cause of serious damage during the 2018 Hokkaido Eastern Iburi Earthquake, we observed microtremors and aftershocks at a landslide area and around strong ground motion observation stations. Subsurface velocity structures were determined using a heuristic approach based on a forward calculation using the phase velocities and H/V spectra. As a result, S-wave velocity structures were estimated, and the predominant frequencies of the H/V spectra were obtained. The predominant frequencies of the H/V spectra of the microtremor and seismic waves are 0.8–5 Hz. The S-wave velocity of the uppermost layer is 75–130 m/s, and its thickness is approximately 10 m. In particular, it has been suggested that the uppermost layer of volcanic ash caused the landslide in the town of Atsuma. The predominant frequency corresponds to the thickness of the alluvial layers with S-wave velocities of 75–300 m/s. It was also found that the predominant direction of the horizontal earthquake ground motion of the landslide was affected by the topography of the mountain.

Keywords: Microtremor, S-wave velocity, The 2018 Hokkaido Eastern Iburi Earthquake, Landslide

1. INTRODUCTION

The 2018 Hokkaido Eastern Iburi Earthquake occurred in the eastern Hokkaido Iburi district, and a seismic intensity of 6+ was recorded at several locations, including the towns of Atsuma, Abira, and Mukawa [1]. According to the seismic intensity distribution map estimated by the Japan Meteorological Agency, a seismic intensity of 6+ or 7 was estimated over a wide area in the eastern region of Hokkaido Iburi [2]. This earthquake caused widespread landslides near Atsuma near the epicenter. In addition, buildings were locally damaged in Mukawa and Abira [3]. To study the causes of such damage, it is necessary to investigate the subsurface structure and strong ground motion characteristics. Therefore, in this study, we conducted microtremor observations at the site of the landslide, the site of building damage, and the site where a seismic intensity of 6+ or greater was observed. In addition, temporary aftershock observations were also conducted at the landslide site.

2. OBSERVATION

2.1 Microtremor Observation

In this study, the following five points were targeted: the landslide sites in Atsuma (ATM); a damaged building site in Mukawa (MKW1); the JMA observation point Shikanuma, where a seismic intensity of 7 was recorded (SKN); and K-NET observation points HKD126 (MKW2) and HKD127 (OIW), where a seismic intensity of 6+ was recorded. The observation sites are shown on the map in Fig.1.

Microtremor array observations were conducted at all sites. A three-component acceleration-type seismometer (JU410) was used for the observations. JU410 is a device that can record microtremors with a period of 0.05–10 s. During the array observation, four seismometers were used, one at the center of the circle and three along the circumference at equal intervals. Each device was synchronized using a GPS clock. The sampling frequency for the measurement was 200 Hz, and the observation time was 15 min. The array radii were 1 m for ATM, MKW1, MKW2, and OIW, and 1 and 4 m for SKN. At the landslide site, one seismometer was installed at the mountainside (ATM_T) and another was installed at the foot (ATM_B) of the mountain. At this location, the sampling frequency for the measurement was 100 Hz, and the observation time was 10 min. The ATM_B was installed at almost the same position as the array observation point (ATM), and the ATM_T was installed near the seismograph used in the seismic observation described later.

2.2 Temporary Seismic Observation

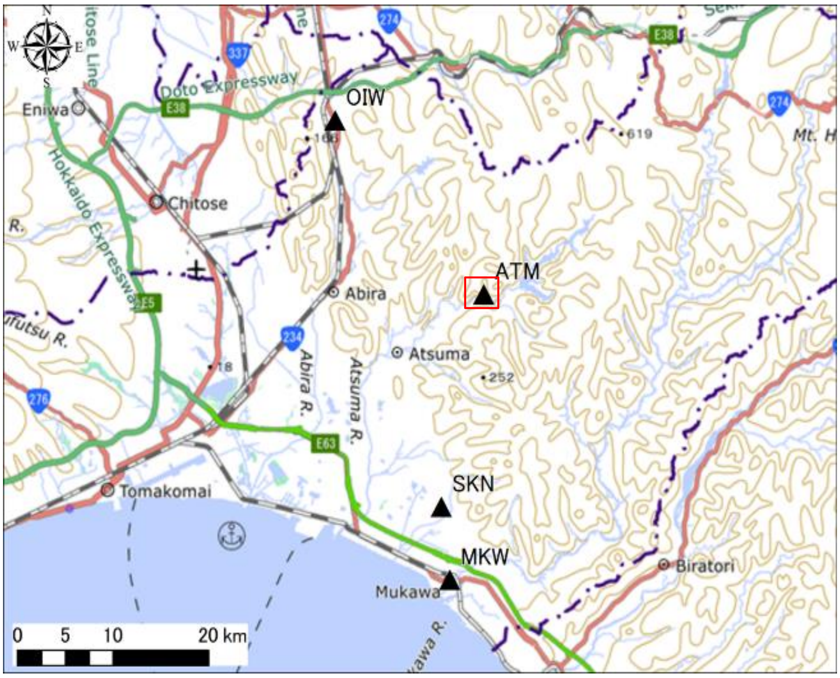

Fig. 1 Locations of the observations (red lined area is shown in close-up in Fig. 5)

Temporary seismic observations were carried out on November 7 and 8, 2018 at the landslide site of Atsuma. For the seismic observation, we used a system in which a three-component velocity seismometer (KVS300) was connected to the data recorder (HKS9700) by a cable. The seismograph was buried near ATM_T on the mountainside where no landslide occurred. The specifications of the observation included a continuous recording at a sampling frequency of 200 Hz, time calibration with a GPS clock, and a battery drive. Three earthquakes were recorded during the temporary observation period. The specifications of the observed earthquakes are listed in Table 1. The observation points are shown in Fig. 5.

3. ANALYSIS

3.1 Microtremor Observation Data

For the analysis of the three-component single-site observation data, 20.48 s periods without artificial noise were selected from the array observation records. The horizontal-to-vertical spectral ratio (H/V spectrum) was calculated using the averaged Fourier spectra of the selected data for each component. The horizontal components were then composed. The spectra were smoothed using a log-window [4] with a coefficient of 20. The H/V spectra of each site are shown in Fig. 2.

For the array observation data, Using the open analyzing tool [5], the phase velocity dispersion curves were estimated based on the CCA method [6]. The conditions for the analysis are as follows: At least five sections were selected through an automatic extraction using the RMS value of the microtremor record of each seismograph with a segment length of 10.24 s. The power spectrum of these sections was smoothed using a Parzen window with a bandwidth of 0.3 Hz and then averaged. Using the power spectrum of each seismograph, the phase velocity dispersion curve was obtained based on the CCA method [6]. The dispersion curves of the phase velocity are shown in Fig. 3.

The velocity of the structures was determined using forward calculations based on borehole data of PS-logging of K-NET and KiK-net (NIED) and geological situations [7]. We determined the subsurface structures to satisfy the H/V spectra and the dispersion curves of the phase velocity by using the fundamental mode of Rayleigh waves within the frequency range of 2–40 Hz. The parameters of the subsurface structure models are the number of layers, density, P-wave velocity Vp, S-wave velocity Vs, and the layer thickness. Densities were set referring previous research in Japan [8], and P-wave velocities were set from S-wave velocities [9]. The physical property values of the subsurface structure models are listed in Table 2. The S-wave velocity structures are shown in Fig. 4.

3.2 Seismic Observation Data

The data processing is as follows: 10.24 s sections of the S-wave part of each component were cut out

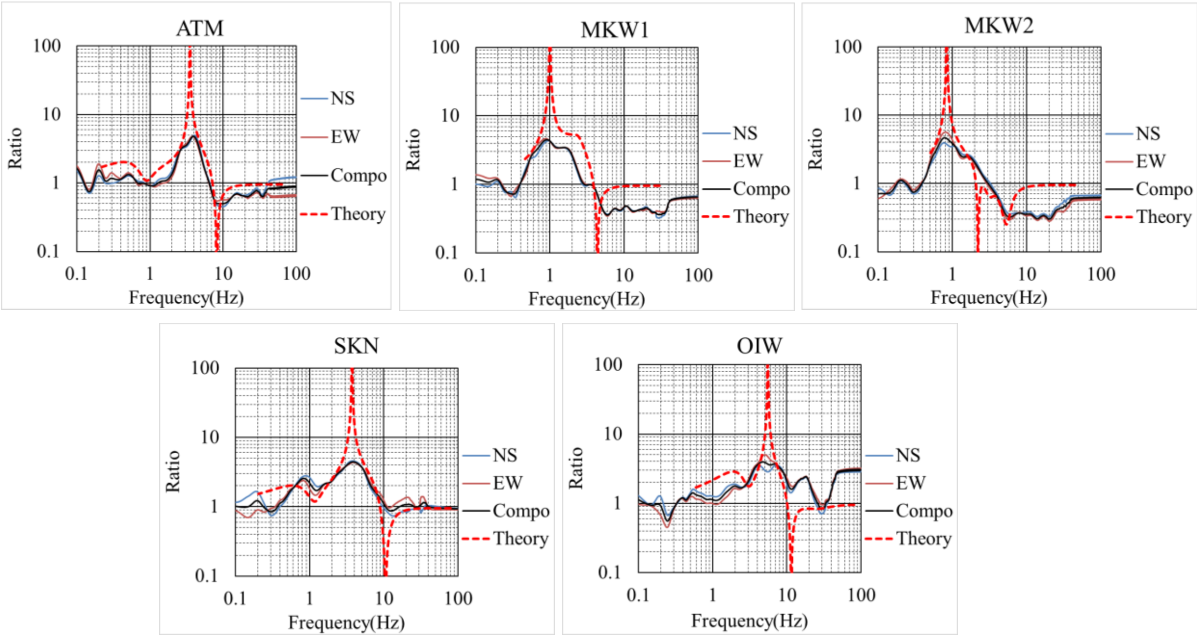

Fig. 2 H/V spectra of microtremors (NS, North-South; EW, East-West; Comp, composition, where the red dashed lines are the theoretical values of the Rayleigh waves using the subsurface structural model)

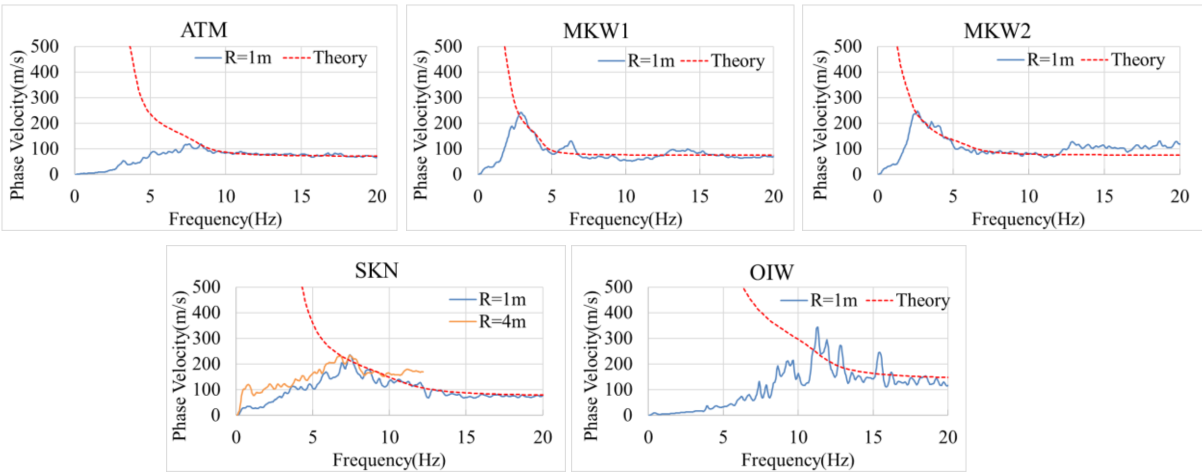

Fig. 3 Dispersion curves of phase velocity (solid lines are curves obtained for each radius. Red dashed lines are the theoretical values of the Rayleigh waves using the subsurface structural model)

from the seismic record, and after applying a cosine taper with a half cycle of 0.5 s to both ends, zero data were added to the 20.48 s period. The Fourier spectrum of each component was calculated by smoothing using a Parzen window with a bandwidth of 0.2 Hz. The H/V spectra were calculated from the Fourier spectra of these three components.

4. RESULTS

4.1 Microtremor H/V Spectra

As a feature of the H/V spectra, there is a clear peak at all points (Fig. 2). The predominant frequencies of the H/V spectra are 3.96 Hz for ATM, 0.78 Hz for MKW1, 0.93 Hz for MKW2, 3.86 Hz for SKN, and 4.79 Hz for OIW. The detailed situation of the H/V shape is as follows. There is a small peak at 1.14 Hz in SKN and a small peak at near 1.5 Hz in MKW1. In addition, a phenomenon occurs in which the shape near the peak differs for OIW.

4.2 S-wave Velocity Structures

The S wave velocity structure at each point is as follows (Table 2, Fig.4). The layer thickness of the soft soil layer (Vs = 80–300 m/s) is described. The layer thickness of the very low-velocity layer at Vs = 80 (75) m/s is 3–9 m (OIW = zero). The maximum

Table 1 Specifications of observed earthquake

Date and time	Latitude	Longitude	Depth	Magnitude
11/08/2018 0:54:32.2	42°33.7′ N	141°56.2′ E	24km	Mj 3.2
11/08/2018 11:15:13.4	42°13.7′ N	141°23.5′ E	104km	Mj 3.7
11/08/2018 11:34:24.8	42°47.1′ N	142°0.5′ E	37km	Mj 2.7

Table 2 Subsurface structural models

ATM

Thickness (m)	ρ(t/m^3)	Vp(m/s)	Vs(m/s)
4	1.5	1370	75
3	1.6	1460	150
3	1.7	1620	300
60	1.9	1900	550
250	2.1	2070	700
∞	2.2	2620	1200

MKW1

Thickness (m)	ρ(t/m^3)	Vp(m/s)	Vs(m/s)
9	1.2	1380	80
35	1.7	1570	250
80	1.9	1900	550
∞	2.2	2620	1200

MKW2

Thickness (m)	ρ(t/m^3)	Vp(m/s)	Vs(m/s)
6	1.2	1380	80
15	1.5	1460	150
40	1.7	1570	250
40	1.9	1900	550
∞	2.2	2620	1200

SKN

Thickness (m)	ρ(t/m^3)	Vp(m/s)	Vs(m/s)
3	1.5	1380	80
4	1.6	1460	150
6	1.7	1620	300
30	1.9	1900	550
200	2.1	2070	700
∞	2.2	2620	1200

OIW

Thickness (m)	ρ(t/m^3)	Vp(m/s)	Vs(m/s)
2	1.5	1430	130
5	1.6	1470	160
30	1.9	1900	550
60	2.1	2070	700
∞	2.2	2620	1200

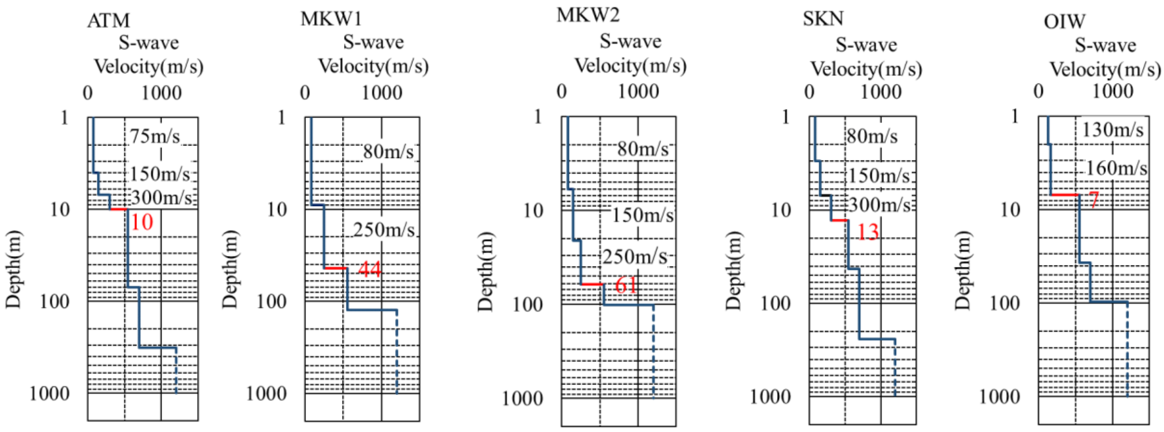

Fig. 4 S-wave velocity structures (black numbers are the S-wave velocities, and the red numbers are the depth to the layer of Vs = 550 ms)

thickness at Vs = 150 m/s and 300 m/s under the first layer is 60 m in Mukawa (MKW1, MKW2), and the thickness of the other sites is 7–10 m. As the g eological condition of this area, the ash layers of the Tarumae volcano are widely distributed [10]. Therefore, it is considered that the first layer of the landslide site (ATM) corresponds to the volcanic ash layer of Tarumae volcano, and that the first layer of the ground model corresponds to the collapsed layer. Layers with S-wave velocities of less than 300 m/s at other points correspond to alluvium or volcanic ash layers. For the soil type of the alluvium, the layers of clay, gravel, and silt are alternated in Mukawa, according to the PS-logging information of K-NET (HKD126). In addition, it was reported that a non-linear ground response occurred at the earthquake observation point (HKD126) in Mukawa [11], which may be related to building damage. In the future, it will be necessary to study the nonlinear ground response based on the ground structure model obtained in this study and to clarify the factors causing the damage.

The deep structure is as follows: The maximum layer thickness at Vs = 550 and 700 m/s layers is 80

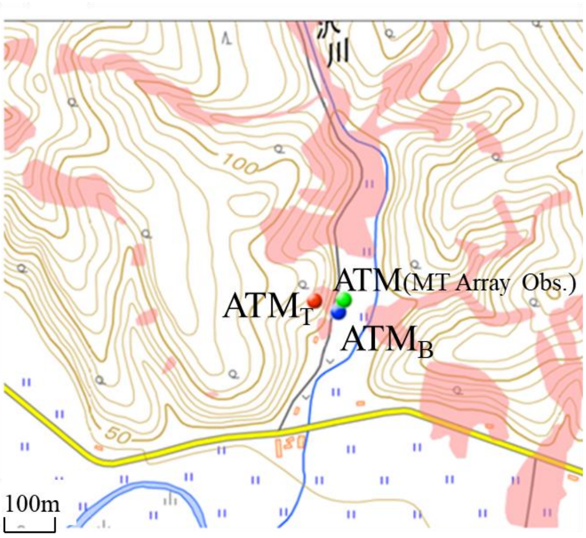

Fig. 5 Location of observation and topographic map at landslide site (orange indicates a landslide area)

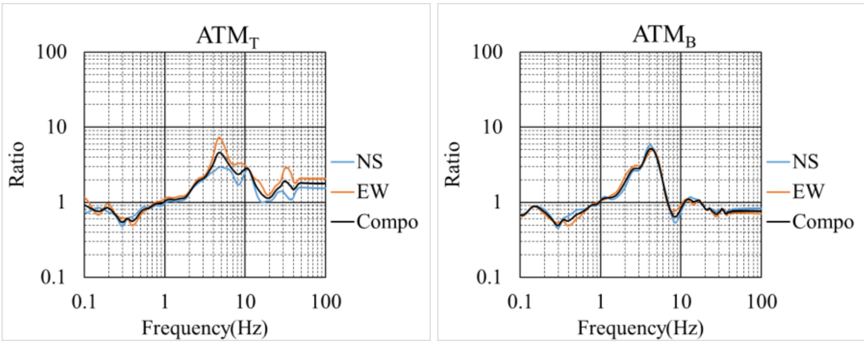

Fig. 6 H/V spectra of microtremor at ATM site

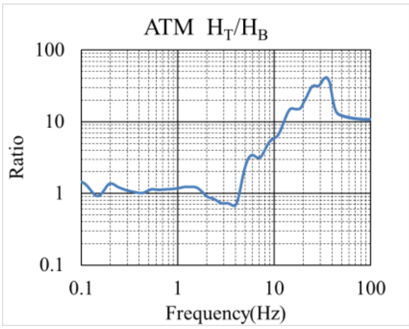

Fig. 7 Horizontal spectral ratio H_T/H_B at ATM site

and 250 m, respectively. The layer at Vs = 550 m/s is considered to correspond to diluvial or volcanic sediments, and the layers at Vs = 700 and 1200 m/s correspond to tuff or Neogene sedimentary rocks. The estimation accuracy is lower than that of the shallow structure model because the dispersion curves of the phase velocity were not sufficiently obtained within the frequency range required for an analysis. However, at Vs = 550 and 700 m/s, the layer thicknesses are reasonable because they are mostly consistent with the previous estimation results [11] of the microtremor observation at HKD126.

4.3 Microtremors at Landslide Site

The location of the observed landslide site is shown on a topographic map in Fig. 5. The area where the landslide occurred (orange area) is

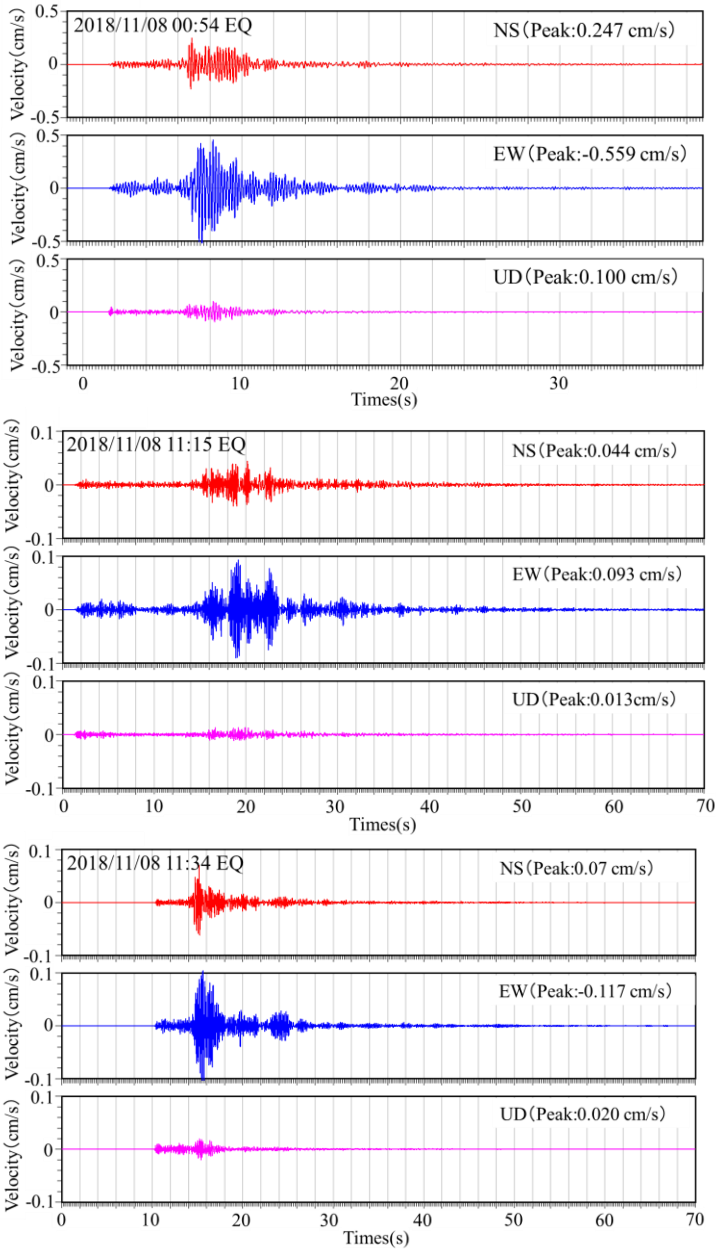

Fig. 8 Velocity waveforms

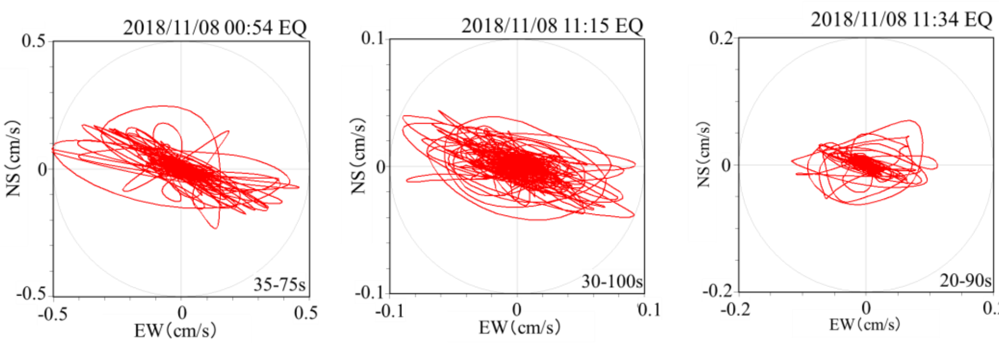

Fig. 9 Particle motions of horizontal components

overlaid on the topographic map, and the tremor observation points used in this study are shown. There are many landslide areas around the target area of this study, and the areas extend along the valleys on steep slopes. The H/V spectra of the ATM_T and foot of the mountain are provided in Fig.

6. The NS component of the horizontal motion is indicated by the blue line, the EW component is shown through the orange line, and the composited value is illustrated by the black line in Fig. 6. A clear peak can be confirmed at approximately 5 Hz at both points. There is a peak near 10 Hz, which is higher than ATM_B within the high frequency band of 4-Hz or more at ATM_T. In addition, although the EW component is larger than the NS component in ATM_T, there are no differences in any components in ATM_B (Fig. 6). The result of calculating the spectral ratio of the horizontal component H_T/H_B (combined values in the NS and EW directions) to the spectrum between both points is shown in Fig. 7. The H_T/H_B gradually increased within the frequency band of 4 to 30 Hz (Fig. 7). From the characteristics of this spectral ratio, it is expected that the seismic motion became larger on the high frequency side of 4 Hz or more than at the foot of the slope.

4.4 Seismic Ground Motions at Landslide Site

The velocity waveforms of the three observed seismic records are shown in Fig. 8. All of these figures are time-series data of velocity of 3 earthquake, with north-south direction: NS on the red line, east-west direction: EW on the blue line, and vertical direction: UD on the pink line. The particle motions of the velocity record of the horizontal component with the NS direction as the vertical axis and the EW direction as the horizontal axis are shown in Fig. 9. The H/V spectra are shown in Fig. 10 (the black line indicates the average of the three earthquake values). The amplitude of the EW component was larger than that of the NS component for all earthquakes (Fig. 8). Not only the peak velocity value but also the amplitude of the entire waveform is large. From the particle motions of the horizontal component, the EW direction is predominant, and the axis of the predominant direction is slightly rotated clockwise (Fig. 9). Furthermore, from the topographic map (Fig. 5) near the observation point, the direction of the slope is almost the same as the predominant direction of the particle motion. As a characteristic of the H/V, the EW component is larger than the NS component near the peak of 5 Hz (Fig. 10). It is possible that such seismic motion characteristics contributed to the landslide. In the future, it will be n ecessary to study the factors that cause these phenomena in more detail and clarify the mechanism of the landslide caused by this earthquake.

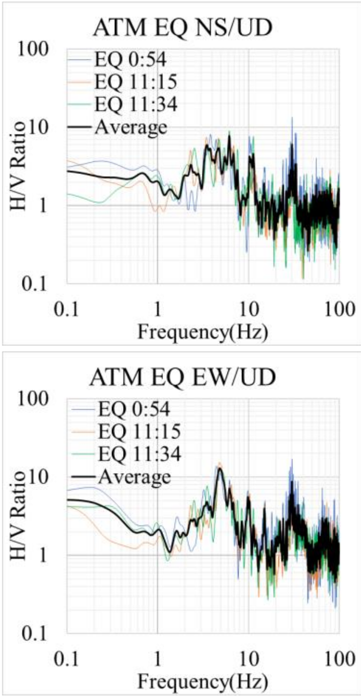

Fig. 10 H/V spectra of earthquakes at ATM

5. CONCLUSIONS

1) In Mukawa, the predominant frequency of the microtremor H/V was 0.8–0.9 Hz, and it was found that the soft soil layers with Vs = 80?300 m/s were thickly deposited in the ground structure. It is considered that this layer amplified the ground motion, and the possibility of a nonlinear response was also suggested.
2) The predominant frequency of the microtremor H/V at other seismic stations was 4 Hz at Shikanuma in the the JMA site of Atsuma, and 5 Hz at the K-NET site HKD127 in Abira. From the ground structure model, it was found that there were soft soil layers at those points and the layer thickness was thinner than that of the K-NET site HKD126 in Mukawa.
3) At the landslide site in Atsuma, the predominant frequency of the microtremor H/V was 5 Hz, and the subsurface structure had a volcanic ash layer with Vs = 75–80 m/s. It is possible that this layer collapsed on the slope near this point.
4) For the characteristics of the microtremors and seismic motions at the landslide site, it was found that the amplitude of the seismic motion

of the EW component was larger at the mountainside than at the foot of the mountain. In addition, it was found that the H/V was larger within the frequency band of higher than 4 Hz in the microtremor, and that the H/V of the EW component was larger than the NE component at near the 5 Hz peak in the seismic ground motion.

In the future, we plan to evaluate the earthquake motion based on the information obtained from the observations. Furthermore, based on the results, we plan to examine the factors causing the strong ground motion and the factors causing the landslide generated by the earthquake.

6. ACKNOWLEDGMENTS

We used seismic intensity information from the Japan Meteorological Agency, and the borehole information on K-NET and KiK-net of the National Research Institute for Earth Science and Disaster Prevention. We used the basic map information of the Geospatial Information Authority of Japan as the base map for the location of the observation points. This work was supported by JSPS KAKENHI Grant Number JP18H01523.

7. REFERENCES

[1] JMA website “Seismic intensity database”, (https://www.data.jma.go.jp/svd/eqdb/data/shindo/Event.php?ID=9901267), (in Japanese).

[2] JMA website “Estimated seismic intensity distribution map, 03:08 on September 06, 2018 Iburi district Middle East M6.7”, (https://www.data.jma.go.jp/svd/eew/data/suikei/201809060308_146/201809060308_146_1.html), (in Japanese).

[3] Cabinet Office Japan website “Disaster management in Japan”, (http://www.bousai.go.jp/updates/h30jishin_hokkaido/pdf/310128_jishin_hokkaido.pdf, (in Japanese).

[4] Konno K. and Ohmachi T., A smoothing function sutable for estimation of amplification factor of the surface ground from microtremor and its application, Journal of JSCE, No.524/1-33, 1995, pp.247-259 (in Japanese with English abstract).

[5] Cho I., Tada T. and Shinozaki Y., Possibility of microtremor array opened up by general theory: Release of analysis tool BIDO, Seismological Society of Japan Fall Meeting in 2009, 2009. (in J apanese)

[6] Cho I., Tada T. and Shinozaki Y., Centerless circular array method: Inferring phase velocities of Rayleigh waves in broad wavelength ranges using microtremor records, Journal of Geophysical Research, 2006, Vo.111, B09315.

[7] National Research Institute for Earth Science and Disaster Resilience, Geo Station (https://www.geostn.bosai.go.jp/), [Viewed on October 9, 2019].

[8] Noguchi T., Nishikawa H., Yoshida S. and Kagawa T., Estimation of subsurface structure and characteristics of ground vibration based on microtremor and seismic observation in the central Tottori Prefecture, Japan, Journal of Japan Association for Earthquake Engineering, Vol. 19, Issue 6, 2019, pp. 258-271. (in Japanese with English abstract)

[9] Kitsunezaki C., Goto N., Kobayashi Y., Ikawa, T., Horike M., Saito T., Kurota T., Yamane K., Okuzumi K., Estimation of P- and S- wave velocities in deep soil deposits for evaluating ground vibrations in earthquake, Natural disaster science, 1990, 9-3, 1-17. (in Japanese with English abstract)

[10] Hirose W., Kawakami G. Kase Y., Ishimaru S., Koshimizu K., Koyasu H. and Takahashi R., Preliminary report of slope movements at Atsuma Town and its surrounding areas caused by the 2018 Hokkaido Eastern Iburi Earthquake, Report of the geological survey of Hokkaido, Vo.90, 2018, pp.33-44 (in Japanese).

[11] Takai N., Shigefuji M., Horita J., Nomoto S., Maeda T., Ichiyanagi M., Takahashi H., Yamanaka H., Chimoto K., Tsuno S., Korenaga M. and Yamada N.: Cause of destructive strong ground motion within 1–2 s in Mukawa town during the 2018 Mw 6.6 Hokkaido eastern Iburi earthquake, Earth, Planets and Space, Vol. 71, 2019, 10.1186/s40623-019-1044-4.